J. Biochem. 2012;151(6):657–666 doi:10.1093/jb/mvs029

JB THE JOURNAL OF BIOCHEMISTRY

Identification of the P-body component PATL1 as a novel ALG-2-interacting protein by *in silico* and far-Western screening of proline-rich proteins

Received January 14, 2012; accepted February 24, 2012; published online March 20, 2012

Kanae Osugi[1], Hironori Suzuki[1,†], Tomomi Nomura[1], Yasuo Ariumi[2], Hideki Shibata[1] and Masatoshi Maki[1,*]

[1]Department of Applied Molecular Biosciences, Graduate School of Bioagricultural Sciences, Nagoya University, Furo-cho, Chikusa-ku, Nagoya 464-8601, Japan; and [2]Center for AIDS Research, Kumamoto University, 2-2-1, Honjo, Kumamoto 860-0811, Japan

*Masatoshi Maki, Department of Applied Molecular Biosciences, Graduate School of Bioagricultural Sciences, Nagoya University, Furo-cho, Chikusa-ku, Nagoya 464-8601, Japan.
Tel: +81-52-789-4088, Fax: +81-52-789-5542,
email: mmaki@agr.nagoya-u.ac.jp

†Present address: Hironori Suzuki, Structural Biology Center, Photon Factory, Institute of Materials Structure Science, High Energy Accelerator Research Organization (KEK), Tsukuba, Ibarakai 305-0801, Japan.

ALG-2 (also named PDCD6) is a 22-kDa Ca^{2+}-binding protein that belongs to the penta-EF-hand family including calpain small subunit and interacts with various proteins such as ALIX and Sec31A at their specific sites containing an ALG-2-binding motif (ABM) present in their respective Pro-rich region (PRR). In this study, to search for novel ALG-2-interacting proteins, we first performed *in silico* screening of ABM-containing PRRs in a human protein database. After selecting 17 sequences, we expressed the PRR or full-length proteins fused with green fluorescent protein (GFP) in HEK293T cells and analysed their abilities to bind to ALG-2 by Far-Western blotting using biotinylated ALG-2 as a probe. As a result, we found 10 positive new ALG-2-binding candidates with different degrees of binding ability. For further investigation, we selected PATL1 (alternatively designated Pat1b), a component of the P-body, which is a cytoplasmic non-membranous granule composed of translation-inactive mRNAs and proteins involved in mRNA decay. Interactions between endogenous PATL1 and ALG-2 proteins were demonstrated by a co-immunoprecipitation assay using their specific antibodies. Furthermore, in immunofluorescence microscopic analyses, PATL1 as well as DCP1A, a well-known P-body marker, co-localized with a subset of ALG-2. This is the first report showing interaction of ALG-2 with a P-body component.

Keywords: calcium-binding protein/motif/P-body/proline-rich/protein–protein interaction.

Abbreviations: aa, amino acids; ABM, ALG-2-binding motif; CBB, Coomassie brilliant blue R-250; FW, far-Western; GFP, green fluorescent protein; GST, glutathione-*S*-transferase; IgG, immunoglobulin G; mAb, monoclonal antibody; NP-40, Nonidet P-40; pAb, polyclonal antibody; PAGE, polyacrylamide gel electrophoresis; PEF, penta-EF-hand; PMSF, phenylmethylsulfonyl fluoride; PVDF, polyvinylidene difluoride; PRR, proline-rich region; WB, western blotting.

ALG-2 (also named PDCD6, programmed cell death 6) was identified as a pro-apoptotic factor in T-cell hybridoma and named after apoptosis-linked gene 2 (*1*). Although no abnormal phenotypes appeared in ALG-2 knockout mice (*2*), accumulating data suggest involvement of ALG-2 in apoptosis in cultured mammalian cells (*3–5*), cell cycle (*6*), signal transduction (*7–10*) and cancer (*11–12*). However, details of its physiological functions have remained unclear. ALG-2 is a 22-kDa Ca^{2+}-binding protein containing five serially repetitive EF-hand motifs (penta-EF-hand, a PEF domain) and belongs to the PEF family including calpain small subunit (*13*, *14*). Upon binding to Ca^{2+}, ALG-2 changes its conformation (*15*) and interacts with various proteins, such as ALIX (*16*, *17*), annexin A11 (*18*), annexin A7 (*19*), Sec31A (*20*, *21*), TSG101 (*22*), PLSCR3 (*23*) and Scotin (*4*). These proteins each contain a proline-rich region (PRR) that is essential for interaction with ALG-2. Generally, PRRs in proteins are flexible and accommodate binding sites for various interacting proteins (*24–26*). Indeed, we previously identified ALG-2-binding sites in the PRRs of ALIX (*27*), Sec31A (*28*) and PLSCR3 (*23*). Comparison of these binding sequences and X-ray crystal structure analyses of ALG-2/ALIX peptide complex as well as apo-ALG-2 revealed two ALG-2-binding motifs: ABM-1, PPYP(x)$_n$YP (x, variable; $n=4$ in ALIX and PLSCR3); ABM-2, PxPGF (x, variable; Sec31A and PLSCR3) (*29*, *30*). Notably, PLSCR3 contains both ABM-1 and ABM-2. While ALG-2$^{\Delta GF122}$ (an alternatively spliced shorter isoform lacking Gly^{121}Phe^{122}) (*30–32*) does not bind to ALIX, it binds to Sec31A and PLSCR3 (*21*, *23*), supporting the presence of two different modes of interactions between ALG-2 and its binding partners. In this study, to search for new ALG-2-interacting proteins, we performed *in silico* screening based on these previous findings: two types of ABMs in PRRs.

After selecting promising candidates for novel ALG-2-interacting proteins, we performed binding assays by expressing each PRR or full-length protein fused with green fluorescent protein (GFP) in HEK293T cells followed by immunoprecipitation

and far-Western (FW) blotting with biotinylated ALG-2 as a probe. Among the positive proteins, we focused on PATL1 (also named Pat1b), a well-known component of the P-body that is a cytoplasmic non-membranous granule composed of translation-inactive mRNAs and proteins involved in mRNA decay (*33*, *34*). PATL1 has ABM-2 and we confirmed interaction between GFP-PATL1 and both isoforms of ALG-2 fused with glutathione-*S*-transferase (GST) by pull-down assays. Furthermore, we showed co-immunoprecipitation of endogenous PATL1 and ALG-2 in a Ca^{2+}-dependent manner and partial co-localization of ALG-2 and PATL1 at P-bodies by indirect immunofluorescence microscopic analyses using specific antibodies, indicating that PATL1 is a novel ALG-2-interacting protein.

Materials and Methods

Antibodies and reagents

The following antibodies were purchased: rabbit anti-GFP serum suitable for immunoprecipitation (Catalog No. A-6455, Invitrogen/Molecular Probes, Carlsbad, CA, USA), mouse anti-GFP monoclonal antibody (mAb; clone B-2, Santa Cruz Biotechnology, Santa Cruz, CA, USA), mouse anti-DCP1A mAb (clone 3G4, Abnova, Taipei, Taiwan) and mouse Sec31A mAb (clone 32, BD Biosciences, Franklin Lakes, NJ, USA). Affinity purification of rabbit anti-human ALG-2 polyclonal antibody (pAb) using the recombinant ALG-2 protein immobilized on an *N*-Hydroxysuccinimide (NHS) column was described previously (*21*). Anti-human ALG-2 antiserum was also raised in a goat using recombinant ALG-2 protein as an antigen, and antibody was similarly affinity-purified. Anti-human PATL1 antisera were raised in rabbits using a PATL1 C-terminal region (450–770 aa) protein (PATL1Ct) that was fused with GST as an antigen, and specific antibodies were affinity-purified using PATL1Ct fused with maltose-binding protein (MBP).

In silico screening

A database search for ABM-containing protein sequences was performed by 'XaaRR-Scan', a custom-made programme (Maze Inc., Tokyo, Japan) that was designed to find a segment containing motifs of interest in a region rich in specified amino acid residues. Protein sequences containing PRR and ABM-1 or ABM-2 were searched for under the following conditions: Query Amino Acid(s), P; Window Size, 20; Slide Size, 1; Content Threshold (%), 25; Minimum Segment Size, 30; Sequence (s) in Segment for ABM-1 (PPYP, P*x*YP, PYP, YP$(x)_{3\text{-}5}$YP) and for ABM-2 (P*x*PGF, P*x*PGW); database, UniProt/SwissProt (http://www.uniprot.org/). Each scoring value of an ABM-1 type motif was defined as follows: PPYP [5], PxYP [3], PYP [3], YP*xxxx*YP [5], YP*xxx*YP [3] and YP*xxxxx*YP [3]. The total score of each protein selected by XaaRR-Scan was calculated by summation of individual motif scores.

Plasmid construction

Human cDNAs of proteins with high XaaRR-Scan scores were purchased from Open Biosystems (Lafayette, CO, USA) or obtained by PCR-cloning from human cDNA libraries with a KOD-Plus-Ver.2 DNA polymerase (Toyobo, Osaka, Japan) using specific primers (Supplementary Table S1), and the cDNAs of full-lengths or fragments encoding PRRs were inserted between the EcoRI site and the SalI site of pEGFP-C3 using an In-Fusion Advantage PCR Cloning Kit (Clontech). Construction of pGFP-Alix and that of pEGFP-C1/hPLSCR3N (1–78 aa) were described previously (*23*, *35*). pmEGFP-C3/HsSec31A.L1 was derived from pFLAG-Sec31A (*21*). Construction of pmEGFP-C2/annexin VII and that of pAnx11Nt-EGFP will be described elsewhere. A human cDNA of PATL1 encoding 1–123 aa was obtained from a human embryonic kidney (HEK) 293 cell cDNA library by the PCR method using specific primers (5′-atactcgagccccaagaatgttccgctacga-3′ and 5′-gaacttcagatccatcccag-3′) designed on the basis of the registered cDNA sequence (NCBI accession number NM_152716.2) and inserted into the XhoI/EcoRI site of pEGFP-C1 (pEGFPC1/PATL1 1–123). To construct pEGFP-C1/PATL1 122–363, a cDNA fragment encoding a PRR of PATL1 (122–363 aa) from the cDNA clone MHS1010-99621899 (Open Biosystems) that corresponds to isoform 2 was inserted into the EcoRI/SalI sites of pEGFP-C1. To construct pEGFP-C2/PATL1 363–770 and pEGFP-C1/PATL1 122–770, a 1.2-kb SalI fragment encoding 363–770 aa of PATL1 was inserted into the SalI site of pEGFP-C2 and into the SalI site of pEGFP-C1/PATL1 122–363, respectively. To construct pEGFP-C1/PATL1 1–770 (full length), an XhoI/ EcoRI fragment from pEGFP-C1/PATL1 1–123 was inserted into the XhoI/EcoRI site of pEGFP-C1/PATL1 122–770.

Cell culture and DNA transfection

HEK293T and HeLa SS4 cells (sub-cloned HeLa cells)(*21*) were cultured in DMEM supplemented with 5% fetal bovine serum (FBS), 100 U/ml penicillin and 100 μg/ml streptomycin at 37°C under humidified air containing 5% CO_2. One day after the cells had been seeded and the cells were transfected with the expression plasmid DNAs by the conventional calcium phosphate precipitation method for HEK293T cells or using FuGENE 6 (Roche Applied Science) for HeLa cells.

Immunoprecipitation

HEK293T cells transfected with expression plasmids for GFP and GFP-fused proteins were harvested and washed in PBS (137 mM NaCl, 2.7 mM KCl, 8 mM Na_2HPO_4 and 1.5 mM KH_2PO_4, pH 7.4) and then lysed in buffer T [50 mM Tris–HCl, pH 7.5, 150 mM NaCl, 1.5 mM $MgCl_2$, 0.2% Triton X-100, 0.1 mM pefabloc, 3 μg/ml leupeptin, 1 μM E-64, 1 μM pepstatin and 0.2 mM phenylmethylsulfonyl fluoride (PMSF)]. Supernatants obtained by centrifugation at 10,000*g* were incubated with rabbit anti-GFP antiserum at 4°C for 1 h. Then the supernatants were incubated with Protein G Sepharose (GE Healthcare Japan, Tokyo) at 4°C for 1 h. After the beads had been recovered by low-speed centrifugation (700*g*) for 1 min and washed in lysis buffer T, the immunoprecipitation products were subjected to SDS–PAGE followed by western blot (WB) analysis and Far-Western (FW) blot analysis.

In the case of immunoprecipitating endogenous PATL1 with rabbit anti-PATL1 pAb, cells were lysed with buffer H [20 mM HEPES–NaOH, pH 7.4, 142.5 mM KCl, 1.5 mM $MgCl_2$, 0.2% Nonidet P-40 (NP-40), 0.1 mM pefabloc, 3 μg/ml leupeptin, 1 μM E-64, 1 μM pepstatin and 0.2 mM PMSF], and either $CaCl_2$ (final concentration, 100 μM) or EGTA (final concentration, 5 mM) was added to the cleared lysate to examine Ca^{2+}-dependency for interaction with ALG-2. RNase A (final concentration, 125 μg/ml) was also added to exclude potential RNA-binding protein-dependent indirect interactions with ALG-2. Since Protein G Sepharose beads gave higher background signals of ALG-2, Dyna beads Protein G (Invitrogen/Life Technologies Japan, Tokyo) were used, and the beads were collected using a magnetic stand and washed with lysis buffer H containing 100 μM $CaCl_2$ or 5 mM EGTA.

WB and FW blot analyses

Proteins were resolved by SDS–PAGE, transferred to polyvinylidene difluoride (PVDF) membranes (Immobilon-P, Millipore, Bedford, MA, USA), and probed with either specific antibodies for WB or biotinylated ALG-2 (bio-ALG-2) for FW (previously designated bio-ALG-2 overlay assay) essentially as described previously (*18*, *23*). Chemiluminescent signals were detected by a LAS-3000mini lumino-image analyzer (Fujifilm, Tokyo, Japan) using Super Signal West Pico Chemiluminescent Substrate (Thermo Fisher Scientific Inc., IL, USA).

GST pulldown

Pull-down assays using GST-fused ALG-2 were carried out essentially as described previously (*21*, *22*). Briefly, HEK293T cells were transfected with the expression plasmids for GFP-fused proteins, and the cleared lysates prepared using lysis buffer H were incubated with glutathione Sepharose beads carrying GST-ALG-2 for 2 h on ice in the presence of 10 μM $CaCl_2$ and RNase A (final concentration, 125 μg/ml). Then the beads were pelleted by low-speed centrifugation and washed three times with lysis buffer H containing 10 μM $CaCl_2$. The proteins bound to the beads were subjected to SDS–PAGE followed by WB.

Immunofluorescence microscopic analysis

Immunostaining was performed essentially as described previously (*36*). Briefly, HeLa cells (2×10^4) were seeded on 18 mm × 18 mm cover slips in dishes of 3 cm in diameter, washed in PBS, fixed in 4% (w/v) paraformaldehyde in PBS at 4°C for 1 h, and then permeabilized in 0.1% Triton X-100 in PBS at room temperature for 5 min. After blocking with 0.1% (w/v) gelatine in PBS at room temperature for 1 h, the cells on the cover slips were incubated with primary antibodies at 4°C overnight and then with secondary antibodies (Alexa Fluor 488-labelled donkey anti-goat immunoglobulin G (IgG), Alexa Fluor 555-labelled donkey anti-rabbit IgG and Alexa Fluor 647-labelled donkey anti-mouse IgG) at room temperature for 1 h. Finally, they were mounted with anti-fading solution [100 mM Tris–HCl, pH 8.5, 25% (w/v) glycerol, 10% (w/v) Mowiol 4–48] and analysed under a confocal laser-scanning microscope FV1000-D equipped with a 60×, 1.35 numerical aperture (NA) oil-immersion objective (UPLSAPO60XO, Olympus, Tokyo, Japan). Fluorescence intensities were quantitatively analysed with ImageJ, a Java-based image processing program developed at the National Institutes of Health and freely available online (http://rsb.info.nih.gov/ij/). For analysis of transiently expressed GFP-PATL1 in HeLa cells, goat anti-ALG-2 pAb and Alexa Fluor 555-labelled donkey anti-goat IgG were used as primary and secondary antibodies, respectively, and fluorescence was analysed with LSM5 PASCAL equipped with a 63×, 1.40 NA oil-immersion objective (Plan-APOCHROMAT 63×/1.40 Oil, Carl Zeiss, Oberkochen, Germany).

Results

In silico screening of new ALG-2-interacting proteins

For searching a database, we used modified motifs of ABM-1 [PPYP, P*x*YP, PYP and YP(x)$_{3-5}$YP] based on the variability in the identified or predicted ALG-2-binding sites in ALIX, PLSCR3, annexin A7 (ANXA7) and annexin A11 (ANXA11). Furthermore, since the substitution of Phe[49] with Trp in PLSCR3 increased the binding ability (data not shown), P*x*PGF/W was assigned as ABM-2. We searched a human protein database in UniProt/SwissProt with the custom-made XaaRR-Scan programme under the following conditions: presence of ABM-1 or ABM-2 in a segment of PRR longer than 30 aa and containing 25% or more of Pro. A total of 246 ABM-1-type proteins (258 segments) and 36 ABM-2-type proteins (37 segments) were extracted from 20,332 entries. After scoring the extracted sequences, we arbitrarily selected 8 proteins with high scores from the ABM-1 type and 10 proteins with potential physiological functions of interest from the ABM-2 type. Since SHISA4 has both motifs of ABM-1 and ABM-2, we selected a total of 17 candidates for *in vitro* binding assays (Supplementary Table S2 for their annotations).

FW analyses

To investigate direct interactions between ALG-2 and the selected candidates, we expressed GFP-fused proteins encoding only a PRR fragment or the full length in HEK293T cells, immunoprecipitated them with anti-GFP antiserum, and performed FW blot analyses using biotinylated ALG-2 (bio-ALG-2) as a probe. As shown in each lower panel of Fig. 1A–D, signals of GFP-fused proteins [PRR fragment (-p); full-length (-f)] were detected in similar intensities by WB analyses of the immunoprecipitates in each series of experiments. In contrast, signal intensities of FW were variable (upper panels). While no signal was observed for GFP used as a negative control (ctrl), positive signals with different intensities were observed for four ABM-1-type proteins (CHERP-p, GRINA-p, MISS-f and VPS37C-p), five ABM-2-type proteins (BCL9-p, LITFL-f, PATL1-p, RBBP6-p, SYVN1-p and TFG-p) and one ABM-1 plus ABM-2-type protein (SHISA4-p) in addition to the previously known ALG-2-interacting proteins (ALIX, ANXA7, ANXA11, Scotin, PLSCR3, Sec31A and RBM22; Fig. 1A–D). Signals stronger than or similar to those for ALIX and Sec31A, which were used as positive controls, were detected for CHERP-p, VPS37C-p and PATL1-p (Fig. 1A–D and Supplementary Table S2 for semi-quantitative evaluation). Since the signal of GFP-PATL1-p overlapped with the non-specific signal of IgG heavy chain (Fig. 1D, upper panel, single asterisk), we re-examined the ability of PATL1 to interact with ALG-2 by over-expressing GFP-fused full-length PATL1 (PATL1-f) and compared with GFP-Sec31A-f (positive control), GFP-RBM22-f and unfused GFP (negative control). In Fig. 1E, regardless of similar intensities in WB signals of GFP (ctrl) and GFP-PATL1-f (lower panel), the FW signal for PATL1-f showed signal intensity similar to that of GFP-Sec31A-f (upper panel). The strongest FW signal was observed for RBM22 (RNA-binding motif 22, regulating splicing process; Fig. 1A and E). Montaville *et al.* (*37*) isolated RBM22 as an ALG-2-interacting protein by yeast two-hybrid screening and demonstrated that over-expression of RBM22-EGFP (enhanced GFP) caused nuclear translocation of co-expressed ALG-2 fused with monomeric red fluorescent protein (mRFP) in NIH3T3 cells, but interaction between the two proteins was not evaluated by biochemical analyses yet.

Identification of ALG-2-binding region in PATL1

We selected PATL1 for further analyses. It has a long PRR (residue No. 155–338; Pro, 24.5%) in the first half of the primary structure and contains a sequence (307-QMLPPAPGFRAFFSA-321; ABM-2, underlined) similar to those of the second ALG-2-binding sites in PLSCR3 and Sec31A (Fig. 2A). To determine whether this 15-residue ABM-2-containing sequence is sufficient for direct binding of PATL1 to ALG-2, we constructed expression vectors encoding this region as well as the full-length and truncated mutants of PATL1 that were fused with GFP and performed FW using bio-ALG-2. While signals of bio-ALG-2 binding were readily detected for the constructs encoding 1–770 (full length) and 122–363 containing a PRR, the signals for the construct encoding 307–321 were detected only after a longer exposure regardless of similar or stronger WB signals (Fig. 2B). Since FW analysis of GFP fused with a short segment containing ABM-2 of PATL1 showed weak ability to interact with ALG-2 compared with the entire PRR, regions other than ABM-2 in PRR may also contribute to interaction with ALG-2. No signals were detected for unfused GFP (ctrl) and for a degraded fragment of GFP-PATL1 363–770 (~32 kDa) under the condition used.

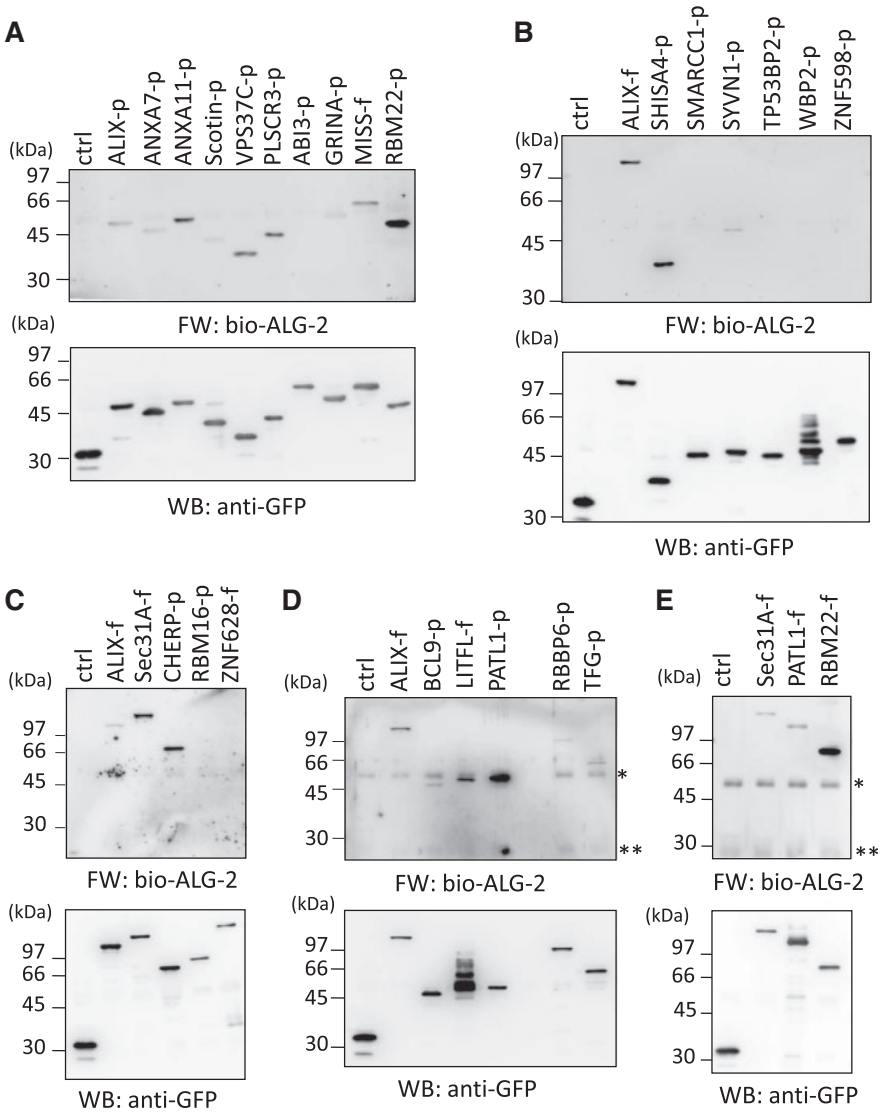

Fig. 1 FW blot analyses of ALG-2-interacting proteins with biotinylated ALG-2. HEK293T cells were transfected with expression vectors for GFP (used as a negative control, ctrl) or each candidate of GFP-fused ALG-2-interacting proteins. At 24 h after transfection, cells were lysed with buffer T (see 'Materials and Methods' section) by gentle mixing (A–D) or by sonication (E), and the supernatants (cleared lysates) obtained after centrifugation at 10,000*g* for 10 min were immunoprecipitated with a rabbit anti-GFP serum. The immunoprecipitates were resolved by SDS–PAGE and subjected to FW blot analyses using biotinylated ALG-2 (bio-ALG-2; upper panels) and WB analyses using anti-GFP mAb (lower panels). GFP-fusion proteins containing only PRRs and full-length sequences of the analysed human proteins are designated -p and -f after the protein names, respectively (A–D). GFP-fused full-length proteins of Sec31A, PATL1 and RBM22 were similarly analysed (E). Single and double asterisks indicate non-specific binding of bio-ALG-2 to immunoglobulin G (IgG) heavy and light chains, respectively. UniProt accession codes, features and evaluation of abilities to interact with ALG-2 are listed in Supplementary Table S2.

GST pull-down assays

There exists an alternatively spliced minor isoform of ALG-2 lacking $Gly^{121}Phe^{122}$ (designated ALG-$2^{\Delta GF122}$; the longer major isoform being designated wild-type, WT, for convenience) (*30–32*). Since Sec31A and PLSCR3 (ABM-2-containing proteins) bind both ALG-2^{WT} and ALG-$2^{\Delta GF122}$, we investigated whether PATL1 and RBM22 also bind ALG-$2^{\Delta GF122}$ by GST pull-down assays using GFP-PATL1 and GFP-RBM22 in the presence of 10 μM $CaCl_2$ (Fig. 3). GST (negative control), GST-ALG-2^{WT} and GST-ALG-$2^{\Delta GF122}$ were immobilized to glutathione Sepharose beads in molar excess of GST over the amount of GST-ALG-2 [Coomassie brilliant blue R-250 (CBB) staining, lower panel]. Proteins pulled down from the lysates (pull-down products) were analysed by WB with anti-GFP mAb. There were no detectable signals in the pull-down products of GST. As expected, signals of GFP-PATL1 were detected in the pull-down products of both GST-ALG-2^{WT} and GST-ALG-$2^{\Delta GF122}$. Unexpectedly, however, signals were barely detectable for GFP-RBM22 even in the pull-down products of GST-ALG-2^{WT} as in the case of unfused GFP (negative control, ctrl).

Co-immunoprecipitation of endogenous PATL1 and ALG-2

Since anti-PATL1 antibody was not commercially available, we raised rabbit anti-PATL1 antisera and affinity-purified pAb, which could be used for WB,

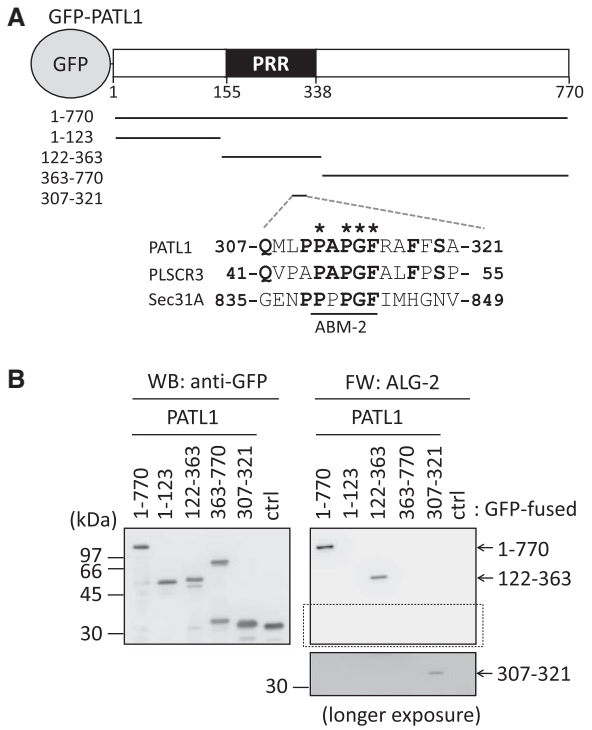

Fig. 2 Identification of the ALG-2-binding site in PATL1. (A) A schematic diagram of GFP-fused PATL1 and its deletion mutants expressed transiently in HEK293T cells. The PRR is indicated by a closed box. Numbers indicate fragments of PATL1 fused with GFP. A segment containing an ABM-2 has a consensus sequence of P*x*PGF (marked with asterisks above the sequence) that is found in the minimal binding regions of PLSCR3 and Sec31A. Identical residues found in these regions of PATL1, PLSCR3 and Sec31A are represented in bold face. (B) FW blot analysis was performed as described in Fig. 1. Exposure time in chemiluminescence detection is 30 s. An image of longer exposure time (300 s) is shown in the right lower panel for the area surrounded by broken line in the upper panel.

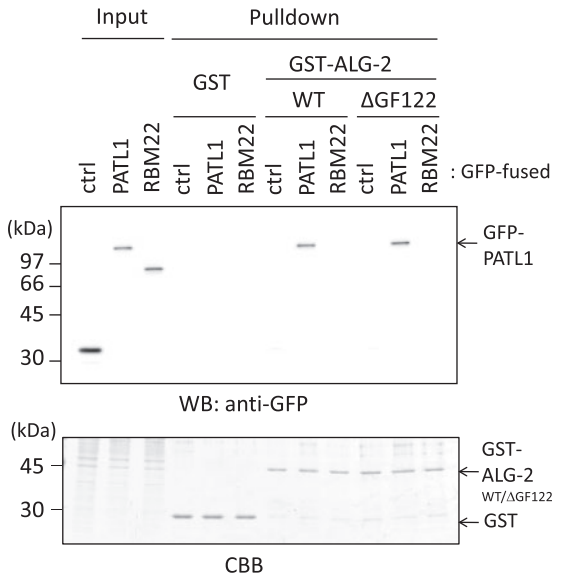

Fig. 3 GST-ALG-2 pull-down assays. HEK293T cells expressing unfused GFP (negative control, ctrl), GFP-PATL1 or GFP-RBM22 were lysed with buffer H. The cleared lysate was treated with RNase A (final concentration, 125 μg/ml) and, after the addition of 10 μM $CaCl_2$, was mixed with glutathione Sepharose beads carrying GST (used as a negative control), GST-ALG-2^{WT} or GST-ALG-2$^{\Delta GF122}$ and incubated for 2 h on ice. Then the beads were pelleted by low-speed centrifugation and washed three times with lysis buffer H containing 10 μM $CaCl_2$. The cleared lysate (Input) and proteins bound to the beads (Pulldown) were subjected to SDS–PAGE, followed either by WB analysis using anti-GFP mAb (upper panel) or by staining with CBB (lower panel). The relative amount of cleared cell lysate proteins (Input) used for analysis of pull-down products was 5%.

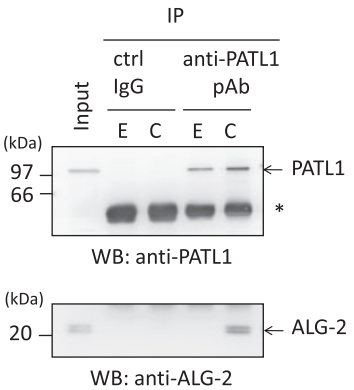

Fig. 4 Co-immunoprecipitation of endogenous PATL1 and ALG-2. HEK293T cells were lysed with lysis buffer T (see 'Materials and Methods' section). After the addition of EGTA to 5 mM (E) or $CaCl_2$ to 100 μM (C), the cleared cell lysate (Input) was subjected to immunoprecipitation by incubating first with either rabbit IgG (used as a negative control, ctrl) or rabbit anti-PATL1 polyclonal antibody (pAb) for 1 h at 4°C and then with magnetic beads carrying Protein G overnight. After the beads had been collected and washed, immunoprecipitated proteins (IP) were resolved by SDS–PAGE and subjected to WB using anti-PATL1 pAb (upper panel) and anti-ALG-2 (lower panel). Asterisk: IgG heavy chain. The relative amount of cleared cell lysate proteins (Input) used for analysis of IP products was 1.5%.

immunoprecipitation and immunofluorescence microscopic analyses. We first investigated whether interaction between endogenous proteins of PATL1 and ALG-2 can be observed in the lysates of HEK293T cells by a co-immunoprecipitation assay, in which immunoprecipitates obtained in the presence of 5 mM EGTA or 100 μM $CaCl_2$ were analysed by WB using respective antibodies for PATL1 and ALG-2. In the upper panel of Fig. 4, a band of ~100 kDa was detected by immunoprecipitation with anti-PATL1 pAb but not with control (ctrl) IgG. Specific doublet bands were detected by WB with anti-ALG-2 pAb in the case of immunoprecipitation with anti-PATL1 pAb in the presence of 100 μM $CaCl_2$ but not in the presence of 5 mM EGTA. No ALG-2 bands were detected in the case of IgG in either condition. It remains unknown whether the faster migrating band observed in the lower panel of Fig. 4 corresponds to the shorter isoform of ALG-2. Occasionally, we observe only a single band. Thus, we cannot exclude the possibility that the observed doublet bands were caused by post-translational modification of ALG-2 by either proteolytic processing or other modifications such as phosphorylation.

Immunofluorescence microscopic analyses

PATL1 is a scaffolding protein of P-bodies that are distributed as non-membranous cytoplasmic foci associated with translation repression and processing of mRNA for degradation (*33*, *34*). Over-expression of GFP-PATL1 in HeLa cells showed punctate distribution by fluorescence microscopic analyses, and fluorescence signals of GFP-PATL1 were merged with those for endogenous ALG-2 as revealed by immunostaining with goat anti-ALG-2 pAb (Supplementary Fig. S1). We performed triple-immunostaining of HeLa cells with rabbit anti-PATL1 pAb and goat anti-ALG-2 pAb together with mouse mAb against either mRNA-decapping enzyme 1A (DCP1A) or Sec31A, a coat component of COPII, which is involved in endoplasmic reticulum (ER)-Golgi vesicular transport. Signals representing ALG-2 were shown as many puncta in the cytoplasm and also as a diffused image in the entire cell including the nucleus (Fig. 5A, panels a and e). On the other hand, observed fluorescent puncta for PATL1 (panels b and f) were merged well with those for DCP1A (panels c and g), but the number of puncta was significantly smaller than the number of puncta representing ALG-2. The punctate signals for PATL1 and DCP1A were merged with those for ALG-2 as shown by arrowheads in the merged images (panels d and h), but fluorescence intensities of ALG-2 in these puncta were weaker than those in other puncta. In Fig. 5B, most of the punctate fluorescence signals of ALG-2 were merged with those of Sec31A (panels i, k and l, open arrowheads), and only a few puncta contained signals of PATL1 (panels i, j and l, closed arrowheads). When fluorescence intensities along the line segment crossing two closely located puncta of PATL1 and Sec31A were quantitatively measured for relative fluorescence intensity with ImageJ (Fig. 5B, panel m, from p_1 to p_2), the value of ALG-2 in PATL1 puncta was ~60% of that in Sec31A puncta (Fig. 5B, panel n).

Discussion

Many non-enzymatic cellular proteins interact with other proteins to regulate their functions, bridge them to other targets as adaptors and form networks to induce various physiological phenomena. ALIX (also previously called AIP1) is the first protein identified as an ALG-2-interacting protein (*16*, *17*). In addition to other previously published ALG-2-interacting proteins (*4*, *18*, *20*, *21*, *23*, *35*), several proteins have been registered as novel ALG-2-interacting partners in online-accessible public interactome databases (*e.g.* BioGRID, http://thebiogrid.org/), which document results of high-throughput yeast two-hybrid or mass spectrometric analyses of affinity-purified proteins with suitable tags that were expressed transiently in cultured cells, but their individual interactions have not been validated by other biochemical methods. To obtain more information on protein–protein interaction networks involving ALG-2, we carried out a semi-large scale screening of novel ALG-2-interacting proteins by different approaches in this study: first, by *in silico* screening of a human amino acid sequence database by finding two types of ALG-2-binding motifs (ABM-1 and ABM-2) in PRRs and then by FW screening of GFP-fused proteins expressed in HEK293T cells using biotinylated ALG-2 as a probe in protein interaction assays. Ten proteins with various potential physiological functions showed positive interactions with different degrees in FW signals (Fig. 1 and Supplementary Table S2). Among these potential targets of ALG-2, we focused on PATL1, which was identified as a human homologue of yeast mRNA decapping activator Pat1 (*33*) and was reported to promote mRNA degradation by connecting deadenylation with decapping (*34*).

To confirm the authenticity of the interaction between ALG-2 and PATL1, we performed interaction analyses employing different methods: (i) GST-ALG-2 pull-down assays (Fig. 3); (ii) co-immunoprecipitation assays using a specific antibody for endogenous PATL1 (Fig. 4); and (iii) immunofluorescence microscopic analyses of subcellular co-localization (Fig. 5). Results of these experiments further support that PATL1 is a genuine ALG-2-interacting protein. On the other hand, physiological interaction between RBM22 and ALG-2 is open to question. Although the strongest FW signals were observed for both PRR and full length of GFP-RBM22 (Fig. 1A and E), GFP-RBM22 was not detected in the pull-down products of GST-ALG-2 (Fig. 3). No signals were detected for endogenous ALG-2 in the immunoprecipitates of GFP-RBM22 (data not shown). Failure in detection of their interaction in cell lysates may be explained as follows: the binding site for ALG-2 is masked by other RBM22-interacting proteins or by itself *in vivo*, but the concealed region is exposed upon SDS- and heat-denaturation during sample treatment for SDS–PAGE preceding FW. We cannot exclude the possibility, however, that exposure of the binding site may occur *in vivo* and RBM22 interacts with ALG-2 under unknown physiological conditions.

Immunofluorescence confocal microscopic analyses have revealed that endogenous ALG-2 is present both in the nucleus and in the cytoplasm (*21*, *27*), where it is distributed in a punctate pattern and mainly localizes to Sec31A-positive ER exit sites (*20*, *21*). Since PATL1 is localized to discrete cytoplasmic foci designated P-bodies (*33*, *34*), we predicted at first that punctate signals of ALG-2 co-localized to PATL1 were as strong as those co-localized to Sec31A. However, in fact, we observed only a modest accumulation of ALG-2 at larger foci of PATL1, and the relative intensity of ALG-2 signal in a PATL1 focus was ~60% of that in Sec31A (Fig. 5B). It is possible that anti-ALG-2 antibody may easily gain access to Sec31A in the ER exit sites but not to PATL1 in P-bodies. Although results of co-immunoprecipitation experiments suggest Ca^{2+}-dependent interaction between ALG-2 and PATL1 (Fig. 4), Ca^{2+}-dependency for subcellular co-localization of the two proteins needs further analyses. Franks and Lykke-Andersen (*38*) suggested that the mRNA decay machinery is limited in a larger P-body that is visible under a microscope, whereas it is unlimited and active under the condition that the P-body remains submicroscopic before aggregation of

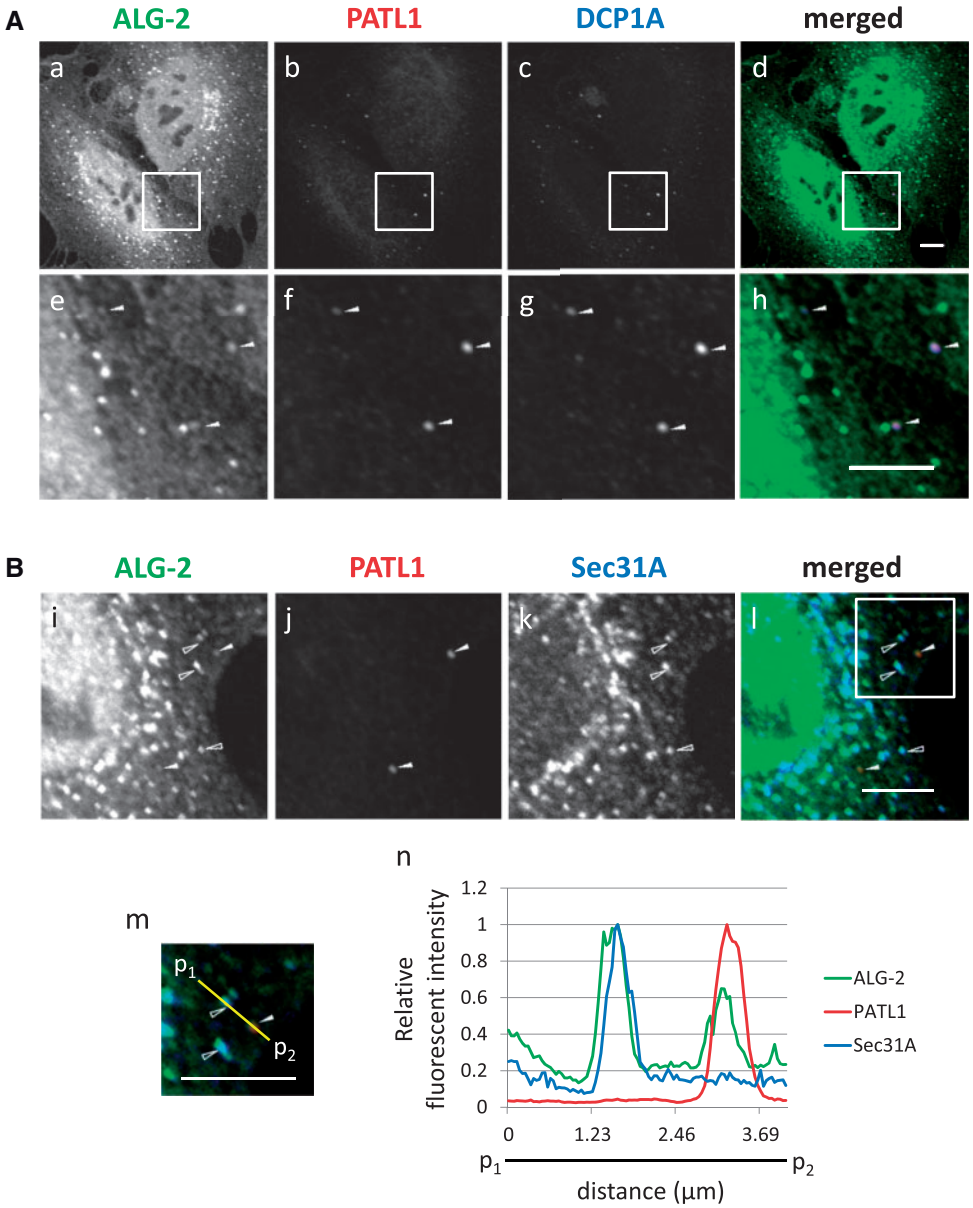

Fig. 5 Punctate subcellular distribution of PATL1 and partial co-localization with ALG-2. HeLa cells were cultured on cover slips, fixed and permeabilized with 0.1% Triton X-100. Then the cells were triple-stained with a goat anti-ALG-2 pAb (green), a rabbit anti-PATL1 pAb (red) and either (A) a mouse anti-DCP1A mAb (blue) or (B) a mouse anti-Sec31A (blue). The fluorescence signals were analysed with a confocal laser-scanning microscope and are represented in black and white. Merged images are shown in (d), (h), (l) and (m). Panels (e–h) and (m) are magnified images of panels (a–d) in A and (l) in B, respectively. Bars: 5 μm. Fluorescence intensities along the line segment (from p_1 to p_2) crossing two puncta indicated by open and closed arrowheads shown in m were measured by ImageJ, and relative fluorescence intensities derived from Alexa Fluor 488 (ALG-2), Alexa Fluor 555 (PATL1) and Alexa Fluor 647 (Sec31A) are represented by green, red and blue curves in a graph (n), where the maximum value is 1.0.

mRNAs with various RNA-binding and -processing proteins. ALG-2 may interact with PATL1 in a state invisible to the microscope during the process of P-body formation or function in other cellular pathways involving PATL1.

PATL1 and its orthologue in yeast are thought to regulate P-body formation (*39*, *40*). The N region in PATL1, corresponding to the PRR, strongly promotes the formation of P-bodies, and PATL1 self-interacts via this region (*34*). Since ALG-2 interacts with PATL1 PRR Ca^{2+} dependent, we hypothesized that ALG-2 is involved in P-body formation by binding to the PRR in PATL1. To test this hypothesis, we carried out co-immunoprecipitation assays with anti-GFP serum using lysates of HEK293T cells transfected with expression vectors of GFP-fused PATL1 and FLAG-tagged PATL1. FLAG-PATL1 was co-immunoprecipitated with GFP-PATL1 even in the presence of 5 mM EGTA, suggesting that Ca^{2+}-dependent binding of ALG-2 to PATL1 does not influence oligomerization of PATL1 (Supplementary Fig. 2). PATL1 and its orthologues associated with

other P-body components such as the decapping enzymes DCP2 and DCP1A and a component of the deadenylation complex (Caf1a) and they are involved in the 5′ to 3′ mRNA decay pathway (*34*, *41–43*). PATL1 and other P-body factors play important roles in effective translation and replication of hepatitis C virus (HCV) RNA (*44*, *45*). Future studies are necessary to determine whether ALG-2 is involved in post-transcriptional control in association with PATL1.

Marnef *et al*. (*46*) recently reported that PATL1 is a nucleocytoplasmic shuttling protein and accumulates in nuclear speckles, foci close to or overlapping with PML bodies and nucleolar caps, suggesting that PATL1 may participate in several RNA-related nuclear processes, such as transcription and splicing, in addition to cytoplasmic gene regulation. Although ALG-2 is present in the nucleus to some extent (*21*, *27*) (Fig. 5A), the mechanism of nuclear translocation remains unclear. ALG-2, 22 kDa as a monomer, may move to the nucleus merely by passive diffusion or may be actively transported to this organelle by association with PATL1 or other proteins of unknown function such as RBM22 (*37*). Although this study did not show the involvement of ALG-2 in the cytoplasmic regulation of gene expression by PATL1, such as translation repression, mRNA degradation and P-body formation, there remains the possibility that ALG-2 and PATL1 play roles in RNA processing or other subnuclear functions within the nucleus. Since ALG-2 functions as a Ca^{2+}-dependent adaptor protein (*30*, *47*), PATL1 might also have a binding partner that associates in the presence of Ca^{2+}-loaded ALG-2. Studies are in progress to search for such partners among the potential ALG-2-interacting proteins that were newly identified in this study.

Supplementary Data

Supplementary data are available at *JB online*.

Acknowledgements

We thank Dr Hitomi, Ms Imoto and other members of the lab for valuable suggestions and discussion. We also thank Dr Stoecklin (German Cancer Research Center) for providing us Pat1b expression plasmids.

Funding

Grant-In-Aid for Scientific Research (B) (General) from Japan Society for the Promotion of Science (JSPS) (20380059, 23380056 to M.M.).

Conflict of interest

None declared.

References

1. Vito, P., Lacana, E., and D'Adamio, L. (1996) Interfering with apoptosis: Ca^{2+}-binding protein ALG-2 and Alzheimer's disease gene ALG-3. *Science* **271**, 521–525
2. Jang, I.K., Hu, R., Lacana, E., D'Adamio, L., and Gu, H. (2002) Apoptosis-linked gene 2-deficient mice exhibit normal T-cell development and function. *Mol. Cell. Biol.* **22**, 4094–4100
3. Rao, R.V., Poksay, K.S., Castro-Obregon, S., Schilling, B., Row, R.H., del Rio, G., Gibson, B.W., Ellerby, H.M., and Bredesen, D.E. (2004) Molecular components of a cell death pathway activated by endoplasmic reticulum stress. *J. Biol. Chem.* **279**, 177–187
4. Draeby, I., Woods, Y.L., la Cour, J.M., Mollerup, J., Bourdon, J.C., and Berchtold, M.W. (2007) The calcium binding protein ALG-2 binds and stabilizes Scotin, a p53-inducible gene product localized at the endoplasmic reticulum membrane. *Arch. Biochem. Biophys.* **467**, 87–94
5. Mahul-Mellier, A.L., Strappazzon, F., Petiot, A., Chatellard-Causse, C., Torch, S., Blot, B., Freeman, K., Kuhn, L., Garin, J., Verna, J.M., Fraboulet, S., and Sadoul, R. (2008) Alix and ALG-2 are involved in tumor necrosis factor receptor 1-induced cell death. *J. Biol. Chem.* **283**, 34954–34965
6. Hoj, B.R., la Cour, J.M., Mollerup, J., and Berchtold, M.W. (2009) ALG-2 knockdown in HeLa cells results in G2/M cell cycle phase accumulation and cell death. *Biochem. Biophys. Res. Commun.* **378**, 145–148
7. Hwang, I.S., Jung, Y.S., and Kim, E. (2002) Interaction of ALG-2 with ASK1 influences ASK1 localization and subsequent JNK activation. *FEBS Lett.* **529**, 183–187
8. Chen, C. and Sytkowski, A.J. (2005) Apoptosis-linked gene-2 connects the Raf-1 and ASK1 signalings. *Biochem. Biophys. Res. Commun.* **333**, 51–57
9. Park, S.H., Lee, J.H., Lee, G.B., Byun, H.J., Kim, B.R., Park, C.Y., Kim, H.B., and Rho, S.B. (2012) PDCD6 additively cooperates with anti-cancer drugs through activation of NF-κB pathways. *Cell. Signal.* In press [PMID:22142513]
10. Rho, S.B., Song, Y.J., Lim, M.C., Lee, S.H., Kim, B.R., and Park, S.Y. (2012) Programmed cell death 6 (PDCD6) inhibits angiogenesis through PI3K/mTOR/p70S6K pathway by interacting of VEGFR-2. *Cell Signal.* **24**, 131–139
11. Yamada, Y., Arao, T., Gotoda, T., Taniguchi, H., Oda, I., Shirao, K., Shimada, Y., Hamaguchi, T., Kato, K., Hamano, T., Koizumi, F., Tamura, T., Saito, D., Shimoda, T., Saka, M., Fukagawa, T., Katai, H., Sano, T., Sasako, M., and Nishio, K. (2008) Identification of prognostic biomarkers in gastric cancer using endoscopic biopsy samples. *Cancer Sci.* **99**, 2193–2199
12. Aviel-Ronen, S., Coe, B.P., Lau, S.K., da Cunha Santos, G., Zhu, C.Q., Strumpf, D., Jurisica, I., Lam, W.L., and Tsao, M.S. (2008) Genomic markers for malignant progression in pulmonary adenocarcinoma with bronchioloalveolar features. *Proc. Natl Acad. Sci. USA* **105**, 10155–10160
13. Maki, M., Narayana, S.V., and Hitomi, K. (1997) A growing family of the Ca^{2+}-binding proteins with five EF-hand motifs. *Biochem. J.* **328,** Pt 2, 718–720
14. Maki, M., Kitaura, Y., Satoh, H., Ohkouchi, S., and Shibata, H. (2002) Structures, functions and molecular evolution of the penta-EF-hand Ca^{2+}-binding proteins. *Biochim. Biophys. Acta* **1600**, 51–60
15. Maki, M., Yamaguchi, K., Kitaura, Y., Satoh, H., and Hitomi, K. (1998) Calcium-induced exposure of a hydrophobic surface of mouse ALG-2, which is a member of the penta-EF-hand protein family. *J. Biochem.* **124**, 1170–1177
16. Missotten, M., Nichols, A., Rieger, K., and Sadoul, R. (1999) Alix, a novel mouse protein undergoing

calcium-dependent interaction with the apoptosis-linked-gene 2 (ALG-2) protein. *Cell Death Differ*. **6**, 124–129

17. Vito, P., Pellegrini, L., Guiet, C., and D'Adamio, L. (1999) Cloning of AIP1, a novel protein that associates with the apoptosis-linked gene ALG-2 in a Ca^{2+}-dependent reaction. *J. Biol. Chem.* **274**, 1533–1540
18. Satoh, H., Shibata, H., Nakano, Y., Kitaura, Y., and Maki, M. (2002) ALG-2 interacts with the amino-terminal domain of annexin XI in a Ca^{2+}-dependent manner. *Biochem. Biophys. Res. Commun.* **291**, 1166–1172
19. Satoh, H., Nakano, Y., Shibata, H., and Maki, M. (2002) The penta-EF-hand domain of ALG-2 interacts with amino-terminal domains of both annexin VII and annexin XI in a Ca^{2+}-dependent manner. *Biochim. Biophys. Acta*. **1600**, 61–67
20. Yamasaki, A., Tani, K., Yamamoto, A., Kitamura, N., and Komada, M. (2006) The Ca^{2+}-binding protein ALG-2 is recruited to endoplasmic reticulum exit sites by Sec31A and stabilizes the localization of Sec31A. *Mol. Biol. Cell.* **17**, 4876–4887
21. Shibata, H., Suzuki, H., Yoshida, H., and Maki, M. (2007) ALG-2 directly binds Sec31A and localizes at endoplasmic reticulum exit sites in a Ca^{2+}-dependent manner. *Biochem. Biophys. Res. Commun.* **353**, 756–763
22. Katoh, K., Suzuki, H., Terasawa, Y., Mizuno, T., Yasuda, J., Shibata, H., and Maki, M. (2005) The penta-EF-hand protein ALG-2 interacts directly with the ESCRT-I component TSG101, and Ca^{2+}-dependently co-localizes to aberrant endosomes with dominant-negative AAA ATPase SKD1/Vps4B. *Biochem. J.* **391**, 677–685
23. Shibata, H., Suzuki, H., Kakiuchi, T., Inuzuka, T., Yoshida, H., Mizuno, T., and Maki, M. (2008) Identification of Alix-type and Non-Alix-type ALG-2-binding sites in human phospholipid scramblase 3: differential binding to an alternatively spliced isoform and amino acid-substituted mutants. *J. Biol. Chem.* **283**, 9623–9632
24. Willamson, M.P. (1994) The structure and function of proline-rich regions in proteins. *Biochem. J.* **297**, 249–260
25. Kay, B.K., Williamson, M.P., and Sudol, M. (2000) The importance of being proline: the interaction of proline-rich motifs in signaling proteins with their cognate domains. *FASEB J.* **14**, 231–241
26. Ren, X. and Hurley, J.H. (2011) Proline-rich regions and motifs in trafficking: from ESCRT interaction to viral exploitation. *Traffic* **12**, 1282–1290
27. Shibata, H., Yamada, K., Mizuno, T., Yorikawa, C., Takahashi, H., Satoh, H., Kitaura, Y., and Maki, M. (2004) The penta-EF-hand protein ALG-2 interacts with a region containing PxY repeats in Alix/AIP1, which is required for the subcellular punctate distribution of the amino-terminal truncation form of Alix/AIP1. *J. Biochem.* **135**, 117–128
28. Shibata, H., Inuzuka, T., Yoshida, H., Sugiura, H., Wada, I., and Maki, M. (2010) The ALG-2 binding site in Sec31A influences the retention kinetics of Sec31A at the endoplasmic reticulum exit sites as revealed by live-cell time-lapse imaging. *Biosci. Biotechnol. Biochem.* **74**, 1819–1826
29. Suzuki, H., Kawasaki, M., Inuzuka, T., Okumura, M., Kakiuchi, T., Shibata, H., Wakatsuki, S., and Maki, M. (2008) Structural basis for Ca^{2+}-dependent formation of ALG-2/Alix peptide complex: Ca^{2+}/EF3-driven arginine switch mechanism. *Structure* **16**, 1562–1573
30. Maki, M., Suzuki, H., and Shibata, H. (2011) Structure and function of ALG-2, a penta-EF-hand calcium-dependent adaptor protein. *Sci. China Life Sci.* **54**, 770–779
31. Tarabykina, S., Moller, A.L., Durussel, I., Cox, J., and Berchtold, M.W. (2000) Two forms of the apoptosis-linked protein ALG-2 with different Ca^{2+} affinities and target recognition. *J. Biol. Chem.* **275**, 10514–10518
32. Inuzuka, T., Suzuki, H., Kawasaki, M., Shibata, H., Wakatsuki, S., and Maki, M. (2010) Molecular basis for defect in Alix-binding by alternatively spliced isoform of ALG-2 (ALG-$2^{\Delta GF122}$) and structural roles of F122 in target recognition. *BMC Struct. Biol.* **10**, 25
33. Scheller, N., Resa-Infante, P., de la Luna, S., Galao, R.P., Albrecht, M., Kaestner, L., Lipp, P., Lengauer, T., Meyerhans, A., and Diez, J. (2007) Identification of PatL1, a human homolog to yeast P body component Pat1. *Biochim. Biophys. Acta* **1773**, 1786–1792
34. Ozgur, S., Chekulaeva, M., and Stoecklin, G. (2010) Human Pat1b connects deadenylation with mRNA decapping and controls the assembly of processing bodies. *Mol. Cell Biol.* **30**, 4308–4323
35. Katoh, K., Shibata, H., Suzuki, H., Nara, A., Ishidoh, K., Kominami, E., Yoshimori, T., and Maki, M. (2003) The ALG-2-interacting protein Alix associates with CHMP4b, a human homologue of yeast Snf7 that is involved in multivesicular body sorting. *J. Biol. Chem.* **278**, 39104–39113
36. Ichioka, F., Kobayashi, R., Katoh, K., Shibata, H., and Maki, M. (2008) Brox, a novel farnesylated Bro1 domain-containing protein that associates with charged multivesicular body protein 4 (CHMP4). *FEBS J.* **275**, 682–692
37. Montaville, P., Dai, Y., Cheung, C.Y., Giller, K., Becker, S., Michalak, M., Webb, S.E., Miller, A.L., and Krebs, J. (2006) Nuclear translocation of the calcium-binding protein ALG-2 induced by the RNA-binding protein RBM22. *Biochim. Biophys. Acta* **1763**, 1335–1343
38. Franks, T.M. and Lykke-Andersen, J. (2007) TTP and BRF proteins nucleate processing body formation to silence mRNAs with AU-rich elements. *Genes Dev.* **15**, 719–735
39. Pilkington, G.R. and Parker, R. (2008) Pat1 contains distinct functional domains that promote P-body assembly and activation of decapping. *Mol. Cell Biol.* **28**, 1298–1312
40. Franks, T.M. and Lykke-Andersen, J. (2008) The control of mRNA decapping and P-body formation. *Mol. Cell* **32**, 605–615
41. Braun, J.E., Tritschler, F., Haas, G., Igreja, C., Truffault, V., Weichenrieder, O., and Izaurralde, E. (2010) The C-terminal alpha-alpha superhelix of Pat is required for mRNA decapping in metazoa. *EMBO J.* **29**, 2368–2380
42. Haas, G., Braun, J.E., Igreja, C., Tritschler, F., Nishihara, T., and Izaurralde, E. (2010) HPat provides a link between deadenylation and decapping in metazoa. *J. Cell Biol.* **189**, 289–302
43. Marnef, A. and Standart, N. (2010) Pat1 proteins: a life in translation, translation repression and mRNA decay. *Biochem. Soc. Trans.* **38**, 1602–1607
44. Scheller, N., Mina, L.B., Galao, R.P., Chari, A., Gimenez-Barcons, M., Noueiry, A., Fischer, U.,

Meyerhans, A., and Diez, J. (2009) Translation and replication of hepatitis C virus genomic RNA depends on ancient cellular proteins that control mRNA fates. *Proc. Natl. Acad. Sci USA*. **106**, 13517–13522

45. Ariumi, Y., Kuroki, M., Kushima, Y., Osugi, K., Hijikata, M., Maki, M., Ikeda, M., and Kato, N. (2011) Hepatitis C virus hijacks P-body and stress granule components around lipid droplets. *J. Virol.* **85**, 6882–6892

46. Marnef, A., Weil, D., and Standart, N. (2012) RNA-related nuclear functions of human Pat1b, the P-body mRNA decay factor. *Mol. Biol. Cell* **23**, 213–224

47. Okumura, M., Ichioka, F., Kobayashi, R., Suzuki, H., Yoshida, H., Shibata, H., and Maki, M. (2009) Penta-EF-hand protein ALG-2 functions as a Ca^{2+}-dependent adaptor that bridges Alix and TSG101. *Biochem. Biophys. Res. Commun.* **386**, 237–241